CHALMERS
UNIVERSITY OF TECHNOLOGY

Millimeter-Wave Array Antenna Architectures Employing Joint Power Combining and Beam Steering for Next-Generation Backhaul Applications

Millimeter-Wave Array Antenna Architectures Employing Joint Power Combining and Beam Steering for Next-Generation Backhaul Applications

Artem R. Vilenskiy*, Sohaib Yaqoob Chaudhry*, Hsi-Tseng Chou†, Marianna V. Ivashina*,
*Antenna Group, Dept. of Electrical Engineering, Chalmers University of Technology, Gothenburg, Sweden
artem.vilenskiy@chalmers.se
†Department of Electrical Engineering, National Taiwan University, Taiwan

***Abstract*—We investigate the capabilities and limitations of joint power-combining and beam-steering techniques for millimeter-wave antenna applications. In this analysis, both functionalities are realized simultaneously through a power-combining and beamforming (PC-BF) network interconnecting an input array of active channels with an array of antenna elements. The first part of the paper provides a review of state-of-the-art hardware architectures of such PC-BF networks and examines their suitability for millimeter-wave applications. The architectures are grouped into two classes depending on the array embedded element patterns properties. Next, a unified PC-BF network is proposed where both functionalities are implemented in a single millimeter-wave waveguiding block. A full-wave model of such a network with 6 inputs and 7 outputs is investigated, with its application demonstrated for a W-band focal-plane array feeding a backhaul reflector antenna.**

***Index Terms*—power combining, beam steering, focal-plane array, mm-wave antennas, wireless backhaul.**

I. Introduction

The problem of high-power generation and radiation in transmitting (TX) radio systems has become especially relevant with increasing industrial focus on high millimeter-wave (mm-wave) frequencies. The emerging civilian mm-wave applications include beyond-5G mobile communication, automotive radars, and sensing [1]. For example, W-band (94 GHz) and D-band (140 GHz) frequencies are currently being considered for next-generation wireless backhaul [2] and base stations of 6G networks, respectively. At the same time, at these frequencies, power generation by existing semiconductor integrated circuit (IC) technologies is quite limited [3] that motivates the utilization of various power-combining techniques. The latter covers a wide spectrum from a simple device-level combining to complicated off-chip 2- and 3-D corporate and spatial combining systems [4]. On the other hand, mm-wave communication transmitters typically employ high-directivity antennas to compensate for a high free-space path loss and achieve a required operation range. Moreover, the beam-steering functionality becomes essential for mm-wave base station antennas aiming at providing wide coverage sectors with spatial multiplexing. The capability to control the antenna beam is nowadays also demanded from extremely high-directivity ($\geq$ 50 dBi) mm-wave backhaul antennas [5]. This is motivated by the requirement to compensate for a dynamic antenna swing due to wind and static pointing errors caused by installation misalignments.

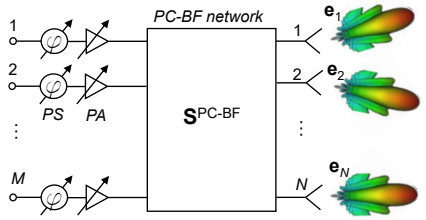

Fig. 1. A general representation of an active antenna system jointly realizing power-combining and beam-steering functionalities through a power-combining and beamforming (PC-BF) network.

Thus, both power-combining and beam-steering functionalities should be implemented in a single TX antenna system, preferably in an integrated manner allowing minimization of lossy system module interconnects. While this problem may look conventional in the case of active phased array antennas, where each array element comprises an active front-end module, for other TX configurations, especially when the number of combined power amplifiers (PAs) M is not equal to the number of radiating elements N, there is still a need for investigation of efficient methods for *joint* power combining and beam steering. Fig. 1 depicts this general case where a linear power-combining and beamforming (PC-BF) multi-port network, described by the S-matrix $\mathbf{S}^{\text{PC-BF}}$, interconnects M active input channels with N radiators. The PC-BF network together with externally phased active sources simultaneously provide power combining and beam steering. Hereinafter, each active channel comprises at least a PA, whereas a phase shifter (PS) is optional, as is the PA's variable gain functionality. We also note that each i-th antenna element may have a unique vector embedded element pattern (EEP) $\boldsymbol{e}_i$.

The first goal of this contribution is to overview and classify existing hardware architectures capable of realizing joint power combining and beam steering, indicating their main features and applicability to mm-wave antenna systems.

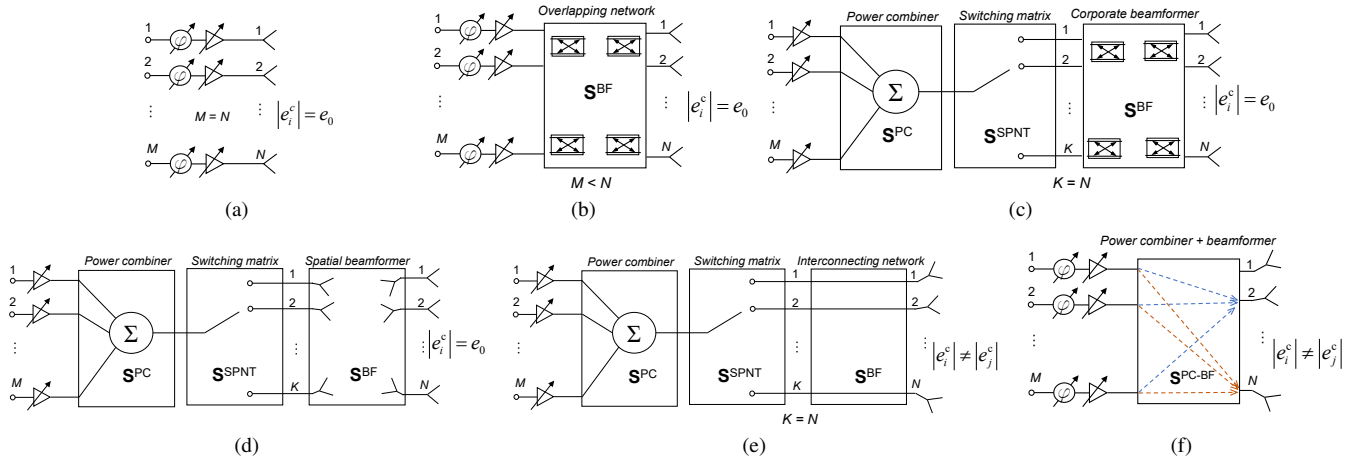

Fig. 2. Various architectures of power-combined active beam-steering antenna systems. Class I, identical EEPs: (a) the conventional phased array architecture; (b) array antennas with sector sub-array patterns; (c) and (d) the modular switched-beam architecture with a corporate and spatial beamformer, respectively. Class II, non-identical EEPs: (e) the modular switched-beam architecture; (f) the architecture based on the unified PC-BF network (proposed).

Next, we propose a unified PC-BF mm-wave network realized as a single block that focuses inward electromagnetic (EM) waves into one of the output channels through a proper phasing of its input excitations. We investigate the performance limitations of such the network as a stand-alone mm-wave component considering a per-port power-combining efficiency and directivity. Finally, we address its quasi-optical (spatial) waveguide implementation and speculate on its applicability in a focal-plane array (FPA) feeding a backhaul reflector antenna.

II. Overview of Available Architectures

Here we propose having a high-level antenna system classification based on the EEP properties. The first class includes antenna systems with identical co-polarized EEP magnitudes (at least in a beam-steering range of interest) $|e_i^{\mathrm{c}}| = e_0, i = 1, ..., N$, where e_i^{c} – the co-polarized EEP of the i-th element. Thus, the second class covers antennas with non-identical EEPs: $|e_i^{\mathrm{c}}| \neq |e_j^{\mathrm{c}}|, i \neq j$. In the following discussion, we will employ the maximum antenna gain criterion, which is commonly used in communication antenna systems [6].

A. Class I: Antenna Systems with Identical EEPs

Antennas of this class are used to generate a high-directivity pencil beam, with beam steering implemented through a variable phase gradient over the aperture. The realized co-polarized antenna gain G_{A} (with input reference planes at the input of antenna elements) can be formulated in the following matrix form:

$$G_{\mathrm{A}} = \frac{\mathbf{a}^* \mathbf{M} \mathbf{a}}{\mathbf{a}^* \mathbf{a}}, \tag{1}$$

where matrix $\mathbf{M} = 4\pi/\eta_0 \mathbf{E}^* \mathbf{E}$, η_0 is the free-space impedance; $\mathbf{E} = [e_1^{\mathrm{c}}, e_2^{\mathrm{c}}, ..., e_N^{\mathrm{c}}]$ is the *row* vector of the co-polarized EEPs; $\mathbf{a}$ is a *column* vector of antenna elements incident complex amplitudes; symbol * denotes the conjugate transpose operation. Dependencies on the spherical coordinates are omitted everywhere for compactness.

Equation (1) can be recognized as the Rayleigh quotient. The solution $\mathbf{a}^{\mathrm{opt}}$ to the problem $\arg\max_{\mathbf{a} \in \mathbb{C}^N} G_{\mathrm{A}}(\mathbf{a})$ is known and represents an eigenvector of $\mathbf{M}$ corresponding to a maximum eigenvalue [6]. Also, it can be analytically shown that $\mathbf{a}^{\mathrm{opt}} = \mathbf{E}^*$, *i.e.*, the optimal beamforming strategy implies the complex conjugate match principle. Since $|e_i^{\mathrm{c}}| = e_0$, to have a maximum realized gain, all antenna elements should be excited uniformly with $\arg(a_i) = -\arg(e_i^{\mathrm{c}})$. Conventional planar and linear active array antennas [Fig. 2(a)] belong to this class (neglecting edge effects). In this case, $M = N$, the PC-BF network is reduced to a direct interconnection between inputs and radiators, while power combining is realized in a free-space manner. If due to imposed design constraints (cost, complexity, *etc.*) we have to reduce the number of active channels ($M < N$), specific PC-BF networks (*e.g.*, Skobelev networks [7]), with S-matrix $\mathbf{S}^{\mathrm{BF}}$, can be used to form M overlapping sub-arrays over the common array aperture [Fig. 2(b)]. Each sub-array is synthesized to have a flat-topped sector EEP suppressing grating lobes due to an oversized sub-array spacing. At the same time, the scan range is typically limited by (15–20)°.

Power combining can also be used with switched-beam antennas [Figs. 2(c), (d)]. For such architectures, a modular approach is commonly utilized. In this case, $\mathbf{S}^{\mathrm{PC\text{-}BF}}$ is formed by (i) a single-output power combiner ($\mathbf{S}^{\mathrm{PC}}$); (ii) a switching matrix or single-pole, N-throw (SPNT) switch with K outputs ($\mathbf{S}^{\mathrm{SPNT}}$); (iii) a beamforming network ($\mathbf{S}^{\mathrm{BF}}$) realizing K antenna beams over the common array aperture. The beamformer can be implemented as a corporate network [Fig. 2(c)], *e.g.*, Butler matrix [8], or in a quasi-optical form [Fig. 2(d)], *e.g.*, Rotman lens [9]. The approach does not employ PSs that represents its main advantage. On another note, the switching matrix, which is typically based on the cascaded switching ICs, introduces a high insertion loss (usually > 3 dB per single switch [5]).

B. Class II: Antenna Systems with Non-Identical EEPs

Well-known examples of this antenna class are FPA-fed reflector and lens antennas [5], [10]. Another example is the

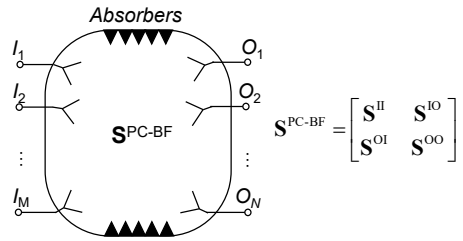

Fig. 3. A quasi-optical implementation of the unified PC-BF network in some waveguiding environment.

conformal switched-beam antennas [11]. In this case, for most practical designs, a switched-beam scenario is realized through a beamformer where elements of an array have a low EEP overlap [6] and thus (1) suggests that only a single element should be effectively excited (however, it may not be the case for dense FPAs [10]). Fig. 2(e) demonstrates the most commonly used PC-BF modular network where switching matrix outputs are directly interconnected with antenna elements ($K = N$). The above-mentioned high insertion loss of the switching matrix noticeably limits system efficiency.

To address the problem of efficiency degradation for this class of active antenna systems we propose using an architecture where a PC-BF network represents a unified mm-wave block. The approach is illustrated in Fig. 2(f). We can also say that the architecture is based on a multiple-output power combiner, where the switching between the outputs is realized by a proper phasing of the input excitations, *i.e.*, the input array of M active channels "focuses" the EM energy into one of N outputs through some EM environment. The obvious advantages of this architecture are reduced insertion loss and system sizes. Below, we investigate its general performance in more detail.

III. Unified PC-BF Networks

A. General Properties

At high mm-wave frequencies, the most attractive implementation of the PC-BF network in Fig. 2(f) is in a quasi-optical (spatial) form since it is less lossy compared with N-way and multi-stage corporate combiners [4]. Also, it greatly simplifies the design when M and N are arbitrary. Fig. 3 schematically shows such a quasi-optical PC-BF structure where EM waves propagate between input (I) and output (O) probes in some waveguiding environment emulating a free space by absorbing a portion of EM energy radiated or bounced towards the structure's sidewalls.

Here, we limit our analysis to the switched-beam case, and therefore we will consider the PC-BF network as a multiple-output combiner switching between N outputs. Similarly to (1), we can formulate the i-th output power-combining efficiency η_i in the Rayleigh quotient form using the input excitation column vector $\mathbf{I}$ and matrix $\mathbf{T} = \mathbf{S}_i^{\mathrm{OI}*}\mathbf{S}_i^{\mathrm{OI}}$, $\mathbf{S}_i^{\mathrm{OI}}$ – the i-th row of the $\mathbf{S}^{\mathrm{OI}}$ submatrix (Fig. 3):

$$\eta_i = \frac{\mathbf{I}^*\mathbf{T}\mathbf{I}}{\mathbf{I}^*\mathbf{I}}. \tag{2}$$

The solution maximizing η_i is $\mathbf{I} = \mathbf{S}_i^{\mathrm{OI}*}$. To describe a relative excitation level of the i-th output when the incident EM power is focused into the j-th channel we introduce directivity D_{ij}:

$$D_{ij} = \frac{(\mathbf{S}_j^{\mathrm{OI}}\mathbf{S}_j^{\mathrm{OI}*})^2}{|\mathbf{S}_i^{\mathrm{OI}}\mathbf{S}_j^{\mathrm{OI}*}|^2},\ i \neq j. \tag{3}$$

Relation (3) shows that a PC-BF network with mutually orthogonal rows of $\mathbf{S}^{\mathrm{OI}}$ will have an ideal directivity. Other performance metrics, such as input channels active reflection coefficient (ARC) and dissipative loss factor, can be found through $\mathbf{S}^{\mathrm{PC\text{-}BF}}$ entries in a conventional way.

It should be emphasized that by maximizing (2) using the complex conjugate match we do not control a power loss distribution between excitation of unwanted output channels (*i.e.*, D_{ij}), ARC, and dissipation in the structure.

B. Uniform Combiners. Performance Limitations

When combining power from M similar PAs, it is desirable to maintain equal drive/compression conditions to have maximum power-added efficiency for all PAs. Therefore, considering the optimal solution of (2), an ideal PC-BF network should have $|S_{ij}^{\mathrm{OI}}| = S_0,\ i = 1, ..., N,\ j = 1, ..., M$, where S_0 is some constant. We will call such PC-BF networks *uniform*. Their performance limitations in terms of S_0 and η are summarized below.

- $M > N$. In this case, $S_0 \leq \sqrt{1/M}$ since $\Sigma_{i=1}^{M}|S_{ij}^{\mathrm{IO}}|^2 \leq 1,\ j = 1, ..., N$. Here, we employ the network reciprocity: $S_{ij}^{\mathrm{IO}} = S_{ji}^{\mathrm{OI}}$. In the limiting case when $S_0 = \sqrt{1/M}$ the maximum achievable combining efficiency becomes $\eta^{\max} = 1$. At the same time, we notice that PC-BF network outputs should be ideally matched and decoupled, *i.e.*, $\mathbf{S}^{\mathrm{OO}} = 0$, and $\mathbf{S}_i^{\mathrm{OI}}\mathbf{S}_j^{\mathrm{OI}*} = 0,\ i \neq j$.
- $M < N$. By using similar constructions we arrive at $S_0 \leq \sqrt{1/N}$ and $\eta^{\max} = M/N$. Thus, the power-combining efficiency is fundamentally limited when $M < N$. This result is expected since a spatially smaller input array of probes cannot efficiently focus EM waves into all elements of a larger output array (*cf.* angular resolution depending on aperture size in conventional array antennas). We also note that in this case $\mathbf{S}^{\mathrm{II}} = 0$.
- $M = N$. Then $S_0 \leq \sqrt{1/N}$ and $\eta^{\max} = 1$ when $\mathbf{S}^{\mathrm{II}},\ \mathbf{S}^{\mathrm{OO}} = 0$. At lower mm-wave and microwave frequencies, this uniform PC-BF configuration can also be realized using multi-stage corporate combiners based on quadrature or rat-race couplers.

IV. Waveguide Implementation and Application in FPA-Fed Reflectors

A. A W-band H-Plane Spatial PC-BF Network

We will consider the most challenging PC-BF network configuration when $M < N$. Fig. 4 depicts an H-plane waveguide (WG) implementation of the network having an

input array of $M = 6$ ridge WGs with $N = 7$ rectangular WG outputs. The structure has a uniform height of 1.27 mm and was designed for 94 GHz central operation frequency. The quasi-optical part of the network represents a parallel-plate WG loaded in the full-wave simulations with absorbing boundary conditions (ABC) along the sidewalls. Both input and output elements are placed along circular arcs with angular coordinates $\alpha_i^{\mathrm{I/O}}$. The input array should be positioned with an average inter-element spacing of half wavelength or slightly higher to mitigate unwanted higher-order interference maxima during focusing into the edge output elements. The output WG elements, on the contrary, should be positioned at a maximal available inter-element distance to improve combiner directivity and have a wider aperture to effectively capture a spatially distributed focused field generated by the input array. The latter makes the output elements more directive which can be compensated by a local rotation of the WGs.

The EM design of the quasi-optical network starts with its decomposition into stand-alone input and output parts by introducing an auxiliary ABC between them. The first design goal is to minimize entries of both $\mathbf{S}^{\mathrm{II}}$ and $\mathbf{S}^{\mathrm{OO}}$. A fast and efficient approach for that is using a 1-D periodic element model [12] that can give a good first-order approximation of an optimal matching circuit design, which is then fine-tuned in the full-scale input/output EM model. After that, both parts are relatively positioned with a goal to uniformly cover each other with corresponding element embedded fields (*i.e.*, EM fields radiated by each element in the parallel-plate WG environment).

The above-mentioned design process was implemented using Ansys HFSS for the following geometric parameters of the structure. Ridge WG: 1.525 mm total width, 0.48 mm and 0.925 mm ridge width and height, respectively; a single E-plane ridge step matching circuit. Rectangular WG: 2.54 mm width; a single H-plane sidewall step matching circuit. Other parameters: $R_{\mathrm{I}} = R_{\mathrm{O}} = 70$ mm, $D_{\mathrm{I}} = D_{\mathrm{O}} = 57$ mm.

Fig. 5 demonstrates simulated results when the EM energy is focused into the 4-th and 5-th output channels. Note that the 0 dB level for the output signal corresponds to a maximal output power of a single PA. We have also limited the maximal input signal variation by 1 dB. The input channels ARC (< -9 dB) and dissipative loss factor ($< 45\%$) are not presented due to space limitations. Results indicate that for both cases up to 3.5 dB of total input power was lost due to dissipative loss, input ARC, and excitation of the unwanted channels. This value may look high but it is still several times lower than the estimated resulting loss of a multi-stage switching matrix used in the modular PC-BF architecture.

B. An FPA Concept with Integrated PC-BF Network. Simulation Results with a Gaussian Beam Feed Model

To test the proposed PC-BF network in a realistic backhaul antenna system, we considered an FPA-fed W-band parabolic reflector antenna [Fig. 6(a)] with 0.4 m diameter and focal ratio $F/D = 0.4$. At this stage, a simplified FPA radiating element Gaussian beam model was used in TICRA GRASP with a

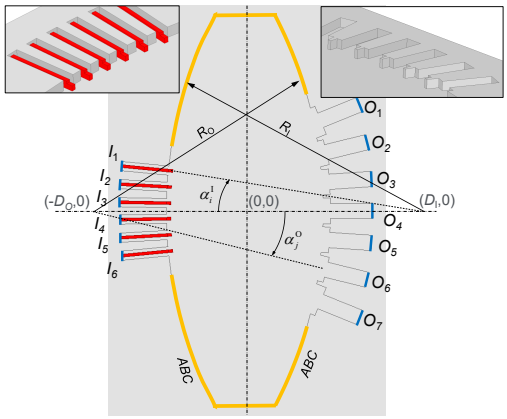

Fig. 4. Geometry of the H-plane PC-BF network with 6 inputs and 7 outputs.

5 dB field taper at the reflector edge. The circular elements arrangement [Fig. 6(a)] realizes around -3 dB crossover level of secondary antenna EEP beams. After obtaining the secondary EEPs, we used the complex conjugate match principle (Section II-A) to synthesize optimal FPA elements excitation coefficients for beam steering at broadside and 0.6° directions. The coefficients, presented in Fig. 6(a), evidence that the FPA has only a single element effectively excited for each beam-steering scenario. Thus, the PC-BF network was used to realize the corresponding power combining in the output ports 4 and 5. The resulting directivity patterns are presented in Figs. 6(b),(c) indicating a very minor main beam directivity loss of < 0.5 dB. This way, the PC-BF network is capable of realizing both required functionalities simultaneously, resulting in high backhaul radio link stability.

V. Conclusion

We have considered several hardware architectures realizing joint power combining and beam steering and categorized them depending on the antenna system EEP properties. When EEPs are non-identical (*e.g.,* in FPA-fed reflector and lens antennas), the most popular modular architecture, employing a switching matrix, becomes extremely lossy at high mm-wave frequencies. This motivated the idea of the proposed unified quasi-optical PC-BF network. We have investigated the general properties and performance limitations of such networks in terms of achievable power-combining efficiency. The early design stage simulation models of the 6-input, 7-output PC-BF network verify the proposed idea and demonstrate the promising performance of the FPA-fed backhaul reflector antenna with the integrated PC-BF network.

Acknowledgment

This work has received funding from the "ENERGETIC" Project supported by VINNOVA (2021-01337) and the Sweden-Taiwan Collaborative Research Framework Project "Antenna Technologies for Beyond-5G Wireless Communication" from the Swedish Foundation for Strategic Research. The authors would like to thank Sam Agneessens, Mingquan Bao, Lars Manholm, Oskar Talcoth (Ericsson AB), Marcus Gavell,

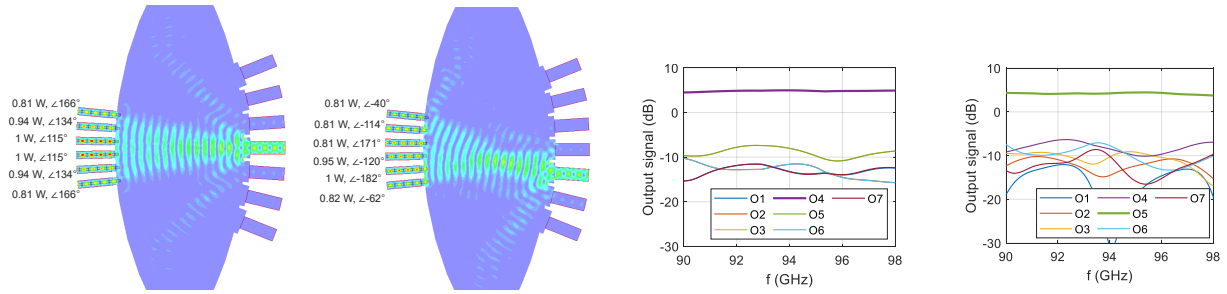

(a) (b) (c) (d)

Fig. 5. Full-wave simulation results of the quasi-optical PC-BF network in Fig. 4: (a), (b) instantaneous distributions of electric surface currents at 94 GHz when focusing the EM energy in the 4-th and 5-th outputs, respectively; (c), (d) corresponding post-processed output signal magnitudes when applying the maximum power-combining efficiency criterion.

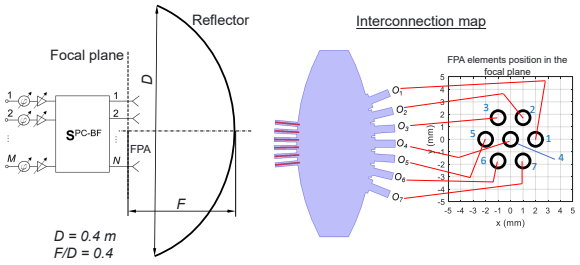

(a)

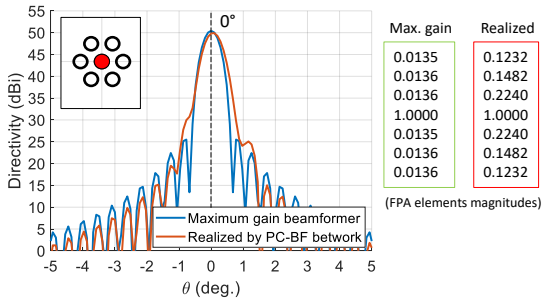

(b)

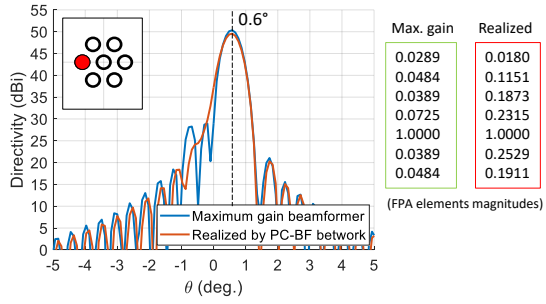

(c)

Fig. 6. (a) Configuration of the FPA-fed reflector antenna and the interconnection map between PC-BF outputs and FPA inputs. Comparison between directivity far-field patterns at 94 GHz for the optimal (maximum gain) and realized by the PC-BF network FPA excitations when scanning the beam at the broadside (b) and 0.6° (c) directions.

Rickard Lövblom, and Göran Granström (Gotmic AB) for their research contributions.

REFERENCES

[1] T. S. Rappaport, Y. Xing, O. Kanhere, S. Ju, A. Madanayake, S. Mandal, A. Alkhateeb, and G. C. Trichopoulos, "Wireless communications and applications above 100 GHz: Opportunities and challenges for 6G and beyond," *IEEE Access*, vol. 7, pp. 78 729–78 757, Jul. 2019.

[2] M. Hörberg, B. Madeberg, D. Sjöberg, H. Zirath, K. Bitsikas, K. Kravariotis, S. Tsapalis, M. Gavell, G. Granström, R. Lövblom, D. Siomos, S. Agneessens, and J. Hansryd, "A W-band, 92–114 GHz, real-time spectral efficient radio link demonstrating 10 Gbps peak rate in field trial," in *2022 IEEE/MTT-S International Microwave Symposium - IMS 2022*, 2022, pp. 545–548.

[3] L. A. Samoska, "An overview of solid-state integrated circuit amplifiers in the submillimeter-wave and THz regime," *IEEE Transactions on Terahertz Science and Technology*, vol. 1, no. 1, pp. 9–24, 2011.

[4] K. Chang and C. Sun, "Millimeter-wave power-combining techniques," *IEEE Trans. Microw. Theory Tech.*, vol. 31, no. 2, pp. 91–107, 1983.

[5] J. Ala-Laurinaho, J. Aurinsalo, A. Karttunen, M. Kaunisto, A. Lamminen, J. Nurmiharju, A. V. Räisänen, J. Säily, and P. Wainio, "2-D beam-steerable integrated lens antenna system for 5G E-band access and backhaul," *IEEE Trans. Microw. Theory Tech.*, vol. 64, no. 7, pp. 2244–2255, 2016.

[6] K. F. Warnick, R. Maaskant, M. V. Ivashina, D. B. Davidson, and B. D. Jeffs, *Phased Arrays for Radio Astronomy, Remote Sensing, and Satellite Communications*, ser. EuMA High Frequency Technologies Series. Cambridge University Press, 2018, ch. 4.

[7] S. Skobelev, "Methods of constructing optimum phased-array antennas for limited field of view," *IEEE Antennas Propag. Mag.*, vol. 40, no. 2, pp. 39–50, 1998.

[8] A. K. Vallappil, M. K. A. Rahim, B. A. Khawaja, N. A. Murad, and M. G. Mustapha, "Butler matrix based beamforming networks for phased array antenna systems: A comprehensive review and future directions for 5G applications," *IEEE Access*, vol. 9, pp. 3970–3987, 2021.

[9] A. Peterson and E. Rausch, "Scattering matrix integral equation analysis for the design of a waveguide Rotman lens," *IEEE Trans. Antennas Propag.*, vol. 47, no. 5, pp. 870–878, 1999.

[10] M. V. Ivashina, O. Iupikov, R. Maaskant, W. A. van Cappellen, and T. Oosterloo, "An optimal beamforming strategy for wide-field surveys with phased-array-fed reflector antennas," *IEEE Trans. Antennas Propag.*, vol. 59, no. 6, pp. 1864–1875, 2011.

[11] V. Semkin, F. Ferrero, A. Bisognin, J. Ala-Laurinaho, C. Luxey, F. Devillers, and A. V. Räisänen, "Beam switching conformal antenna array for mm-wave communications," *IEEE Antennas Wireless Propag. Lett.*, vol. 15, pp. 28–31, 2016.

[12] A. R. Vilenskiy, Y. Zhang, E. Galesloot, A. B. Smolders, and M. V. Ivashina, "Millimeter-wave quasi-optical feeds for linear array antennas in gap waveguide technology," in *2022 16th European Conference on Antennas and Propagation (EuCAP)*, 2022, pp. 1–5.